symmetry

MDPI

Article

Equiauxetic Hinged Archimedean Tilings

Tibor Tarnai [1], Patrick W. Fowler [2,*], Simon D. Guest [3] and Flórián Kovács [1,*]

[1] Department of Structural Mechanics, Budapest University of Technology and Economics, Műegyetem rkp. 3, 1111 Budapest, Hungary; tarnai.tibor@emk.bme.hu
[2] Department of Chemistry, University of Sheffield, Sheffield S3 7HF, UK
[3] Department of Engineering, University of Cambridge, Trumpington Street, Cambridge CB2 1PZ, UK; sdg@eng.cam.ac.uk
* Correspondence: P.W.Fowler@sheffield.ac.uk (P.W.F.); kovacs.florian@emk.bme.hu (F.K.)

Abstract: There is increasing interest in two-dimensional and quasi-two-dimensional materials and metamaterials for applications in chemistry, physics and engineering. Some of these applications are driven by the possible auxetic properties of such materials. Auxetic frameworks expand along one direction when subjected to a perpendicular stretching force. An *equiauxetic framework* has a unique mechanism of expansion (an *equiauxetic mode*) where the symmetry forces a Poisson's ratio of −1. Hinged tilings offer opportunities for the design of auxetic and equiauxetic frameworks in 2D, and generic auxetic behaviour can often be detected using a symmetry extension of the scalar counting rule for mobility of periodic body-bar systems. Hinged frameworks based on Archimedean tilings of the plane are considered here. It is known that the regular hexagonal tiling, $\{6^3\}$, leads to an equiauxetic framework for both single-link and double-link connections between the tiles. For single-link connections, three Archimedean tilings considered as hinged body-bar frameworks are found here to be equiauxetic: these are $\{3.12^2\}$, $\{4.6.12\}$, and $\{4.8^2\}$. For double-link connections, three Archimedean tilings considered as hinged body-bar frameworks are found to be equiauxetic: these are $\{3^4.6\}$, $\{3^2.4.3.4\}$, and $\{3.6.3.6\}$.

Keywords: auxetic; tilings; symmetry; point group

Citation: Tarnai, T.; Fowler, P.W.; Guest, S.D.; Kovács, F. Equiauxetic Hinged Archimedean Tilings. *Symmetry* **2022**, *14*, 232. https://doi.org/10.3390/sym14020232

Academic Editor: Teik-Cheng Lim

Received: 27 November 2021
Accepted: 29 December 2021
Published: 25 January 2022

1. Introduction

Auxetic materials and metamaterials are of technical and theoretical importance, with a spectrum of potential and realised applications [1–6], and they play a pivotal role in the theoretical explanation of rigidity and mobility in periodic systems [7,8]. This is a rapidly growing area of research; for example, if we limit our attention to those proposed metamaterials that are auxetic, the review [1] cites over 270 references relevant to this sub-field. An *auxetic* structure is defined by the initially surprising property of expanding along one direction when stretched along a perpendicular direction [9,10]. There is a considerable literature of experimental, theoretical and modelling work on such structures, e.g., [11–15]. One interesting subset of auxetics consists of those that have symmetric behaviour: *equiauxetic* structures have a Poisson's ratio of −1. Thus, they display the auxetic property for all directions of stretch [16].

A symmetry treatment of mobility in periodic structures [17] has been adapted for the detection of equiauxetic behaviour [16] and applied to an extensive catalogue of 2D bar-and-joint frameworks in which rigid bars along polygon edges *pivot freely* at mutual joints [18]. This symmetry criterion has also been used to study equiauxetic mechanisms in *hinged tilings*: structures where the polygonal tiles of a tessellation of the plane are treated as rigid bodies connected by one, or sometimes more, pin-jointed bars per tile–tile edge contact. The three *regular* tilings of the plane by hexagons, squares and triangles have been studied in this context [19], yielding insight on the extent to which mobility properties of periodic systems can be deduced from finite physical models.

Many tiling-like patterns appear in structural chemistry, and many chemical realisations have been investigated because of the interest in 2D layer materials inspired by the discovery of graphene [20]. Layer materials now have their own journals, e.g., FlatChem, 2D Materials, and 2D Materials and Applications, and the properties of these materials are attracting interest from both theoreticians and experimentalists. One Archimedean tiling made up of carbon atoms appears in the 2D projection of the hypothetical auxetic carbon allotrope, pentagraphene [21,22], and another in the putative superconductor, T-graphene [23]. Some biomaterials can also be modelled as tilings: the regular square tiling appears in an auxetic layer material constructed from self-assembled pin-jointed aldolase tetramers [24]. Other constructions based on tilings connected by hinges have attracted interest in the mathematical literature [25]. Modifications of hinge tilings and lattices in practical application are also of current interest [26–28].

Here we investigate the extension of the symmetry treatment of equiauxeticity to *Archimedean* tilings, which are defined as vertex-transitive, edge-to-edge tilings of the plane with at least two types of regular polygonal tile. Some authors [29] use the term Archimedean inclusively to cover both semi-regular and regular tilings, but here we restrict its use to the non-regular cases. Our tilings are hinged, and in the first case of interest, they have a single link (pin-jointed bar) for each edge of the closed tiling, with one end pinned to each of the rigid contacting tiles, arranged with a consistent sense of rotation for all tiles. Eight such single-link *hinged Archimedean tilings* exist, of which one has mirror-image forms in 2D. Bar lengths are taken to be generic up to symmetry, i.e., equal for symmetrically equivalent edges but otherwise arbitrary. Established symmetry techniques, with extensions to deal with non-transitivity of edges and dependence of mobility counts on unit-cell size, turn out to be informative for these non-regular tilings.

In the earlier work on hinged *regular* tilings [19], both double- and single-link tilings were studied. Double-link connection with equivalent bars imposes an additional condition, in that the edges of neighbouring polygons must remain parallel. Regular tilings are edge-transitive, and the parallel constraint is therefore guaranteed for a totally symmetric expansion. However, of the Archimedean tilings, only the Kagome lattice is edge-transitive. As shown below, results for the mobility of these double-link hinged Archimedean tilings are obtained by minor modification of the character-table calculation for the single-link structure.

Finally, we note that finite analogues of the hinged tilings, the hinged expanding polyhedra (or expandohedra), have been studied in a symmetry context as models for deployable structures that occur in nature and engineering [30,31]. Structures such as cowpea chlorotic mottle virus and dengue virus, respectively, are known to undergo conformational transitions under the influence of changes in pH [32] and temperature [33]. Hinging of rigid subunits gives models for transitions of both types.

2. Theory

2.1. Mobility of Body-Bar Frameworks

The structures considered here are 2D *body-bar* frameworks, consisting of rigid bodies connected by pin-jointed bars. For n bodies connected by b bars, the Tay counting rule [34] gives the net mobility (the number of mechanisms, m, minus the number of states of self-stress, s) in two dimensions as

$$m - s = 3n - 3 - b. \tag{1}$$

This equation for a finite 2D body-bar framework has symmetry-extended version [35]:

$$\Gamma(m) - \Gamma(s) = [\Gamma(v, C) - \Gamma_0] \times (\Gamma_T + \Gamma_R) - \Gamma(e, C), \tag{2}$$

and a further extension to periodic systems [19]

$$\Gamma(m) - \Gamma(s) = \Gamma(v, C) \times (\Gamma_T + \Gamma_R) - \Gamma(e, C) + \Gamma_T \times \Gamma_T - \Gamma_T - \Gamma_R. \tag{3}$$

The detailed reasoning leading to the last equation is given elsewhere [17]; the process is essentially one of allowing for freedoms of the bodies, removing rigid-body motions of the whole lattice, applying the (scalar) constraints imposed by the bars, and excluding motions that are disallowed for a 2D periodic framework.

The notation used in (2) and (3) requires some brief explanation. In 2D, the representations Γ_T and Γ_R refer to the rigid-body motions of frameworks in the plane: the two independent translations within the plane and the single rotation about the normal to the plane. The general notation Γ(object) denotes the reducible representation of a set of objects, consisting of the vector of *characters* $\chi(R)$ in which, for a finite structure, each entry gives the number of objects *unshifted* under operation R. In periodic calculations, the objects counted under a given operation are either unshifted or shifted to translationally equivalent positions. If the objects have vector or tensor characters, the resolution of components onto their original positions must also be considered. The permutation representations $\Gamma(v, C)$ and $\Gamma(e, C)$ describe the symmetries of the vertices and edges of a *contact polyhedron* C [36], which has vertices at body centres and an edge for each bar-constraint linking a pair of bodies.

In the present case, this so-called contact 'polyhedron' is infinite and is combinatorially equivalent to the dual of the tiling, i.e., to a Laves tiling [29]. As in previous work [17], all representations are to be calculated in the finite group $\mathcal{G}$ obtained by factoring out translations from the infinite wallpaper group that describes the 2D periodic structure; the group $\mathcal{G}$ is isomorphic to a point group. The groups $\mathcal{G}$ appropriate to the Archimedean tilings are listed in Table 1.

Table 1. Archimedean tilings and symmetry groups. In the first column, tilings are labelled by the vertex symbol in a nomenclature recommended by [37], which describes the cyclic sequence of faces around a vertex, much as the Schläfli symbol does for polyhedra [38]. The tiling group is the 2D wallpaper group [29], $\mathcal{W}$. The linked tiling belongs to the maximum rotational subgroup, $\mathcal{W}'$. The point group $\mathcal{G}$ is formed by factoring out translations from $\mathcal{W}'$.

Tiling	$\mathcal{W}$	$\mathcal{W}'$	$\mathcal{G}$
$\{3^4.6\}$	$p6$	$p6$	$\mathcal{C}_6$
$\{3^3.4^2\}$	$p2mg$	$p2$	$\mathcal{C}_2$
$\{3^2.4.3.4\}$	$p4mg$	$p4$	$\mathcal{C}_4$
$\{3.4.6.4\}$	$p6mm$	$p6$	$\mathcal{C}_6$
$\{3.6.3.6\}$	$p6mm$	$p6$	$\mathcal{C}_6$
$\{3.12^2\}$	$p6mm$	$p6$	$\mathcal{C}_6$
$\{4.6.12\}$	$p6mm$	$p6$	$\mathcal{C}_6$
$\{4.8^2\}$	$p4mm$	$p4$	$\mathcal{C}_4$

For hinged tilings, on the introduction of links following a consistent sense of rotation, the symmetry is reduced to a pure rotational group, isomorphic to a cyclic group, $\mathcal{G} \cong \mathcal{C}_n$, where n is the order of the principal axis. These groups are abelian but with separable degeneracy and complex irreducible representations for $n > 2$. Standard sets of point-group tables [39–41] are available for the calculation of all the necessary representations. Figure 1 shows for each case: the Archimedean tiling, a portion of that tiling in a partially expanded state along an auxetic pathway, and the dual Laves tiling that corresponds to the infinite 'contact polyhedron'. The figure is drawn for the 'regular' choice of geometry, where all edges are of equal length.

2.2. Equiauxetic Systems

Equation (3) can be applied to periodic systems to give a symmetry condition sufficient for equiauxeticity. The symmetry criterion for equiauxetic behaviour [16] is that the reducible representation for the *net mobility*, $\Gamma(m) - \Gamma(s)$, should include, with positive weight, one or more irreducible representations of $\mathcal{G}$ of A or B type (i.e., non-degenerate,

and hence with character, respectively, $+1$ or -1 under the principal rotation operation in $\mathcal{G}$, which should be of order 3, 4 or 6). These correspond to symmetry-detectable equiauxetic modes. They can be identified by a standard tabular calculation [42], as used below.

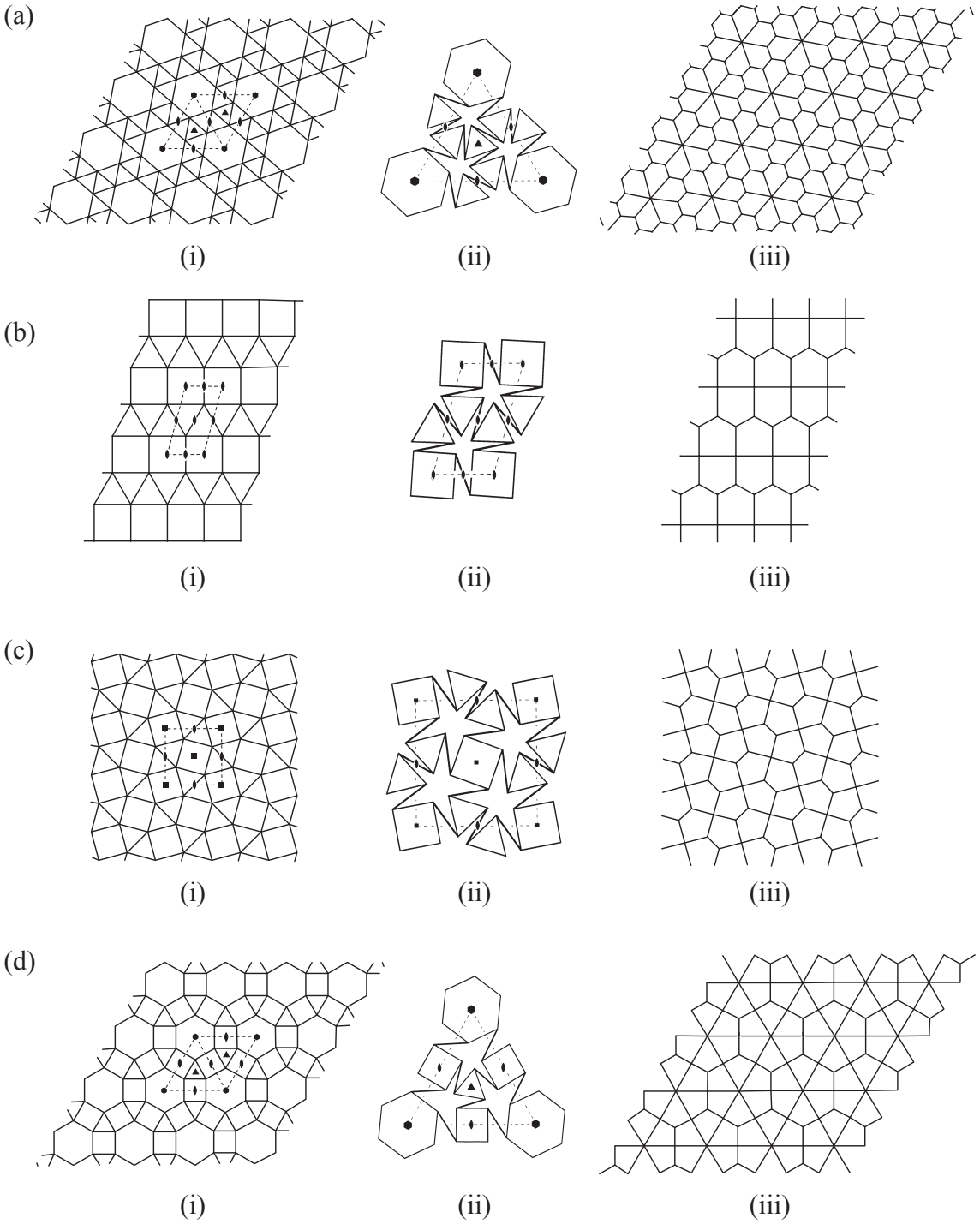

Figure 1. *Cont.*

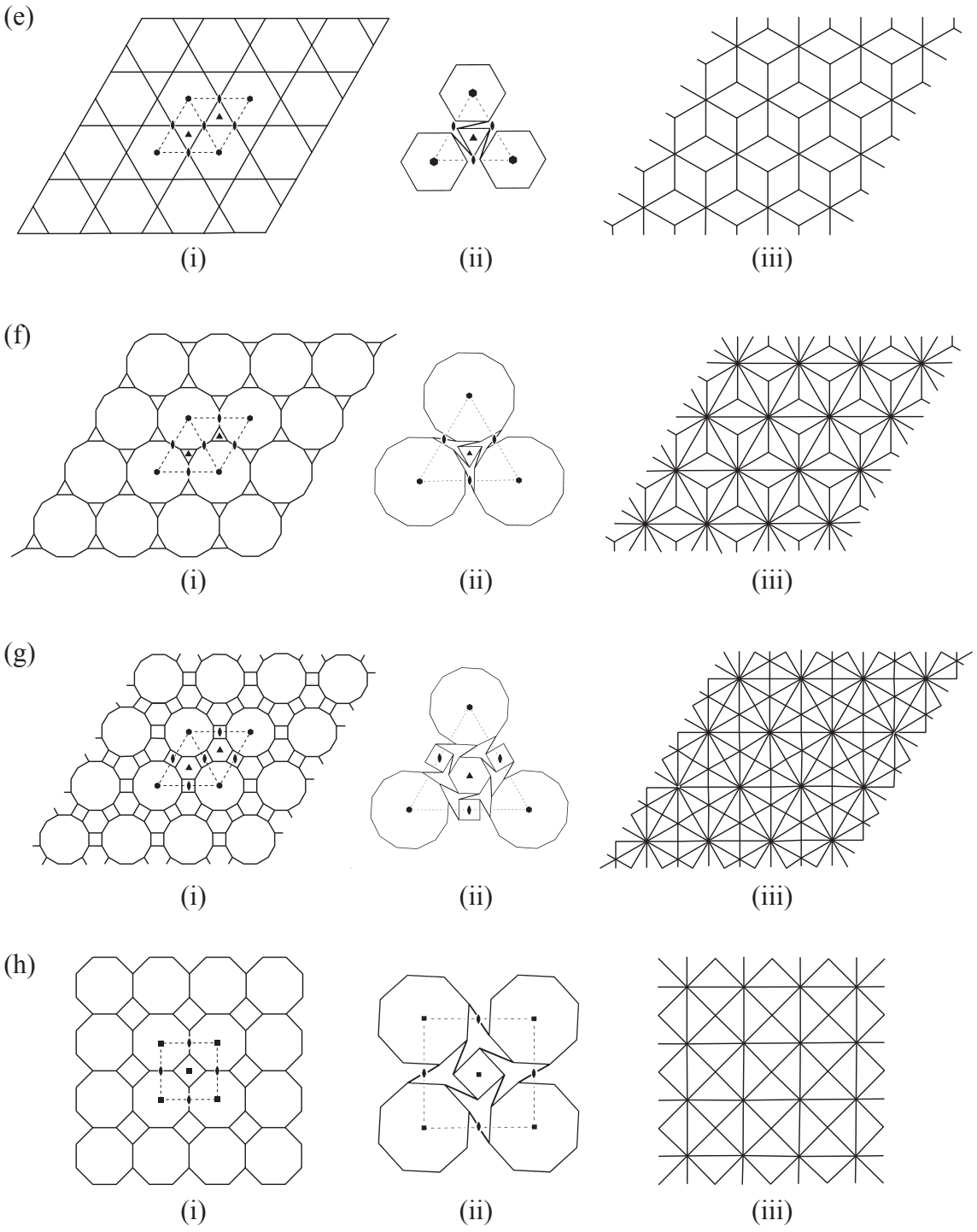

Figure 1. Archimedean tilings and mobility of their *single-link* hinged versions. Panels (**a**–**h**) show (**i**) the closed tiling, (**ii**) a sample of an auxetic expansion mode, and (**iii**) the dual Laves tessellation. Rotational symmetry elements of orders 2, 3, 4, 6 are indicated by conventional symbols ⧫, ▲, ■, ⬢. The order in which tilings are presented in Table 1.

The totally symmetric representation of a group $\mathcal{G}$ is a special case of type A, in that it has character $+1$ under all operations of that group motion along any A or B mode, with the exception of the totally symmetric representation, is a distortion that results in halving of the group, with the result that the distortion mode becomes totally symmetric in the smaller group. The appropriate group $\mathcal{G}$ for some hinged Archimedean tilings turns out to be $\mathcal{C}_2$. Our symmetry condition can never predict equiauxeticity for this case,

as a totally symmetric distortion can have different expansion in orthogonal directions in this symmetry. A totally symmetric mode in $\mathcal{C}_2$ could perhaps be made auxetic by careful tuning.

We note that equations such as (3) predict the *net* mobility $\Gamma(m) - \Gamma(s)$; any mechanisms that are cancelled by equisymmetric states of self-stress are not detectable by this method. Furthermore, if $\Gamma(s)$ contains the totally symmetric representation, the predicted mechanisms of any symmetry might be infinitesimal in nature. In consequence, a mechanism detected by the symmetry criterion can be *guaranteed* finite only if it can be shown that there is no totally symmetric state of self-stress in the reduced symmetry corresponding to that mechanism [43].

We use the terminology of equiauxetic modes and frameworks. An *equiauxetic mode* is a mechanism in which symmetry forces cause uniform expansion of the framework, i.e., a 'breathing' mode. This mode can either maintain the full symmetry of the framework (when it belongs to the totally symmetric irreducible representation) or it may halve the group [16]. We call a framework an *equiauxetic framework* only if the mechanism is an equiauxetic mode. Such a system must deform with a Poisson's ratio of -1.

3. Single-Link Hinged Tilings

For single-link hinged tilings, the mobility count is given by the trace of (3) under the identity operation, i.e.,

$$m - s = 3n - b + 1,$$

as n counts the bodies (tiles), one bar is associated with each of the b edges in the unit cell, and the characters of sets of in-plane translations and rotations are, respectively, $\chi_T(E) = 2$ and $\chi_R(E) = 1$. In the single-link case, the site symmetry of the hinge constraint is that of an edge in the original tiling, subject to the exclusion of any improper symmetry, and is either $\mathcal{C}_2$ or the trivial $\mathcal{C}_1$.

3.1. Calculations

Calculations of the mobility representation $\Gamma(m) - \Gamma(s)$ using Equation (3) are now shown for the eight single-linked Archimedean tilings. In each case, the calculation is carried out for a $k \times k$ array of copies of the basic unit cell indicated in Figure 1. The steps in the calculation are shown in Tables 2–9 for each of the single-link Archimedean tilings. For an explicit example of how characters are calculated, consider Table 2 for tiling $\{3^4.6\}$. The rhomboidal unit cell, shown below in Figure 2a, contains in total one hexagon and eight triangles. At each corner of the cell, a C_6 axis (and hence also C_3 and C_2 axes) passes through the centre of the unique hexagon h; a C_3 axis passes through the centres of triangles t_1 and t_2 in the interior of the cell, and a two-fold axis passes through edge midpoints e_1, at the centre of the cell, and e_2, e_3 at the centres of the cell edges.

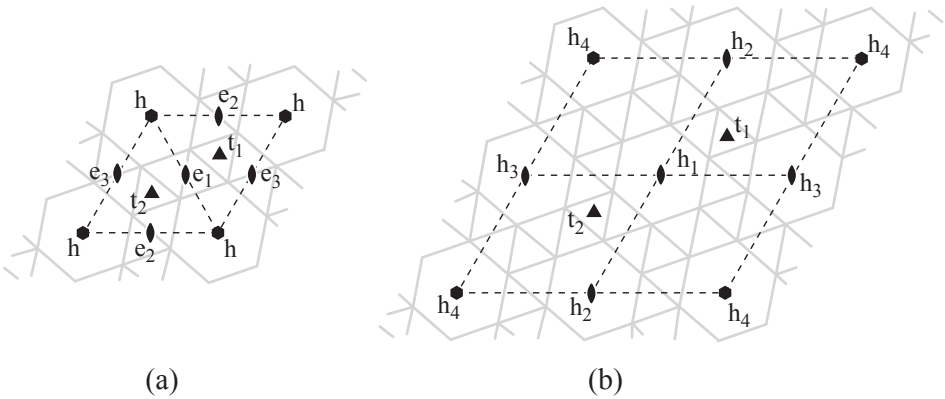

Figure 2. Odd- and even-multiple $k \times k$ unit cells for the $\{3^4.6\}$ tiling: (**a**) $k = 1$; (**b**) $k = 2$.

Table 2. Character calculation for $k \times k$ fragments of single-link hinged tiling $\{3^4.6\}$ (See Figure 1a). The table shows the calculation of the mobility representation $\Gamma(m) - \Gamma(s)$. Entries for rotations and their inverses are equal, as permutation representations $\Gamma(v, C)$ and $\Gamma(e, C)$ are real. Entries under C_2 depend on the parity of k.

Tiling $\{3^4.6\}$, Group $\mathcal{C}_6$	E	C_6	C_3	C_2	
				odd k	**even** k
$\Gamma(v, C)$	$9k^2$	1	3	1	4
$\times(\Gamma_T + \Gamma_R)$	3	2	0	-1	-1
	$27k^2$	2	0	-1	-4
$-\Gamma(e, C)$	$-15k^2$	0	0	-3	0
$+\Gamma_T \times \Gamma_T - \Gamma_T - \Gamma_R$	1	-1	1	5	5
$= \Gamma(m) - \Gamma(s)$	$12k^2 + 1$	1	1	1	1

Table 3. Character calculation for $k \times k$ fragments of single-link hinged tiling $\{3^3.4^2\}$ (See Figure 1b).

Tiling $\{3^3.4^2\}$, Group $\mathcal{C}_2$	E	C_2	
		odd k	**even** k
$\Gamma(v, C)$	$3k^2$	1	4
$\times(\Gamma_T + \Gamma_R)$	3	-1	-1
	$9k^2$	-1	-4
$-\Gamma(e, C)$	$-5k^2$	-3	0
$+\Gamma_T \times \Gamma_T - \Gamma_T - \Gamma_R$	1	5	5
$= \Gamma(m) - \Gamma(s)$	$4k^2 + 1$	1	1

Table 4. Character calculation for $k \times k$ fragments of single-link hinged tiling $\{3^2.4.3.4\}$ (See Figure 1c).

Tiling $\{3^2.4.3.4\}$, Group $\mathcal{C}_4$	E	C_4	C_2	
			odd k	**even** k
$\Gamma(v, C)$	$6k^2$	2	2	4
$\times(\Gamma_T + \Gamma_R)$	3	1	-1	-1
	$18k^2$	2	-2	-4
$-\Gamma(e, C)$	$-10k^2$	0	-2	0
$+\Gamma_T \times \Gamma_T - \Gamma_T - \Gamma_R$	1	-1	5	5
$= \Gamma(m) - \Gamma(s)$	$8k^2 + 1$	1	1	1

Table 5. Character calculation for $k \times k$ fragments of single-link hinged tiling $\{3.4.6.4\}$ (See Figure 1d).

Tiling $\{3.4.6.4\}$, Group $\mathcal{C}_6$	E	C_6	C_3	C_2	
				odd k	**even** k
$\Gamma(v, C)$	$6k^2$	1	3	4	4
$\times(\Gamma_T + \Gamma_R)$	3	2	0	-1	-1
	$18k^2$	2	0	-4	-4
$-\Gamma(e, C)$	$-12k^2$	0	0	0	0
$+\Gamma_T \times \Gamma_T - \Gamma_T - \Gamma_R$	1	-1	1	5	5
$= \Gamma(m) - \Gamma(s)$	$6k^2 + 1$	1	1	1	1

Table 6. Character calculation for $k \times k$ fragments of single-link hinged tiling $\{3.6.3.6\}$ (See Figure 1e).

Tiling $\{3.6.3.6\}$, Group $\mathcal{C}_6$	E	C_6	C_3	C_2	
				odd k	**even** k
$\Gamma(v,C)$	$3k^2$	1	3	1	4
$\times(\Gamma_T+\Gamma_R)$	3	2	0	-1	-1
	$9k^2$	2	0	-1	-4
$-\Gamma(e,C)$	$-6k^2$	0	0	0	0
$+\Gamma_T\times\Gamma_T-\Gamma_T-\Gamma_R$	1	-1	1	5	5
$=\Gamma(m)-\Gamma(s)$	$3k^2+1$	1	1	4	1

Table 7. Character calculation for $k \times k$ fragments of single-link hinged tiling $\{3.12^2\}$ (See Figure 1f).

Tiling $\{3.12^2\}$, Group $\mathcal{C}_6$	E	C_6	C_3	C_2	
				odd k	**even** k
$\Gamma(v,C)$	$3k^2$	1	3	1	4
$\times(\Gamma_T+\Gamma_R)$	3	2	0	-1	-1
	$9k^2$	2	0	-1	-4
$-\Gamma(e,C)$	$-9k^2$	0	0	-3	0
$+\Gamma_T\times\Gamma_T-\Gamma_T-\Gamma_R$	1	-1	1	5	5
$=\Gamma(m)-\Gamma(s)$	1	1	1	1	1

Table 8. Character calculation for $k \times k$ fragments of single-link hinged tiling $\{4.6.12\}$ (See Figure 1g).

Tiling $\{4.6.12\}$, Group $\mathcal{C}_6$	E	C_6	C_3	C_2	
				odd k	**even** k
$\Gamma(v,C)$	$6k^2$	1	3	4	4
$\times(\Gamma_T+\Gamma_R)$	3	2	0	-1	-1
	$18k^2$	2	0	-4	-4
$-\Gamma(e,C)$	$-18k^2$	0	0	0	0
$+\Gamma_T\times\Gamma_T-\Gamma_T-\Gamma_R$	1	-1	1	5	5
$=\Gamma(m)-\Gamma(s)$	1	1	1	1	1

Table 9. Character calculation for $k \times k$ fragments of single-link hinged tiling $\{4.8^2\}$ (See Figure 1h).

Tiling $\{4.8^2\}$, Group $\mathcal{C}_4$	E	C_4	C_2	
			odd k	**even** k
$\Gamma(v,C)$	$2k^2$	2	2	4
$\times(\Gamma_T+\Gamma_R)$	3	1	-1	-1
	$6k^2$	2	-2	-4
$-\Gamma(e,C)$	$-6k^2$	0	-2	0
$+\Gamma_T\times\Gamma_T-\Gamma_T-\Gamma_R$	1	-1	5	5
$=\Gamma(m)-\Gamma(s)$	1	1	1	1

The face centres of the tiling are vertices of the Laves dual, and edge centres in both the tiling and its dual coincide, so the Laves tiling defines the contact polyhedron C. As noted earlier, reducible representations $\Gamma(v,C)$ and $\Gamma(e,C)$ are permutation representations in which the entries count the appropriate structural components unshifted within the unit cell (or moved to translationally equivalent sites in neighbouring cells) by the rotations that comprise point group $\mathcal{G}$. Equivalently, this counting can be achieved by keeping track of the

number of symmetry element symbols that lie within a unit cell (with fractional counting for elements on the cell perimeter). The characters of permutation representations are by definition purely real, even though the separably degenerate *irreducible* representations of cyclic groups have complex characters.

For this tiling, with odd values of k, the entry in $\Gamma(v, C)$ under C_6 is 1 (h preserved); under C_3 it is 3 (h, t_1, t_2 all preserved); under C_2 it is 1 (only h preserved, as no other face of the tiling is pierced by a C_2 axis). The edge representation $\Gamma(e, C)$ has entry 0 for C_6 and C_3 (an edge in a 2D lattice cannot lie on a C_n axis with $n > 2$), and the entry for C_2 is 3 (e_1, e_2, e_3 all preserved). For even values of k, entries under C_6 and C_3 are unchanged, but the entry under C_2 is 4 (h_1, h_2, h_3, h_4 preserved); likewise, the entry in $\Gamma(e, C)$ is now 0 (as no symmetry element passes through an edge). Characters under the identity are trivially equal to the tile counts of $9k^2$ for vertices and $15k^2$ for edges of $\mathcal{C}$, respectively. Hence, as shown in Table 10, the final result for the reducible representation $\Gamma(m) - \Gamma(s)$ is a sum of $(12k^2, 0, 0, 0)$ and $(1, 1, 1, 1)$, i.e., a sum of $2k^2$ copies of the regular representation and one copy of the totally symmetric representation: $A + 2k^2\Gamma_{reg}$.

Table 10. Mobility representations for single- and double-link hinged (regular and Archimedean) tilings. The reducible representation of the net mobility, $\Gamma(m) - \Gamma(s)$, is listed for a $k \times k$ array of copies of the smallest unit cell. Results for the Archimedean tilings follow from Tables 2–9, and those for the three regular tilings are adapted from [19]. Γ_{reg} is the regular representation, with entry $|\mathcal{G}|$ under the identity, and zero under all other operations: Γ_{reg} is $A + B$ in $\mathcal{C}_2$; $A + E$ in $\mathcal{C}_3$; $A + B + E$ in $\mathcal{C}_4$; $A + B + E_1 + E_2$ in $\mathcal{C}_6$.

Tiling	Group	k	Single-Link: $\Gamma(m) - \Gamma(s)$	Double-Link: $\Gamma(m) - \Gamma(s)$
$\{3^6\}$	$\mathcal{C}_6$	odd	$A + B + E_2 + \frac{1}{2}(k^2-1)\Gamma_{\text{reg}}$	$A + E_2 - E_1$
		even	$A + E_2 + \frac{1}{2}k^2\Gamma_{\text{reg}} - E_1$	
$\{4^4\}$	$\mathcal{C}_4$	odd	$A + B + \frac{1}{4}(k^2-1)\Gamma_{\text{reg}}$	$A + B - E - \frac{1}{4}(k^2-1)\Gamma_{\text{reg}}$
		even	$A + \frac{1}{4}k^2\Gamma_{\text{reg}}$	$A - \frac{1}{4}k^2\Gamma_{\text{reg}}$
$\{6^3\}$	$\mathcal{C}_6$	odd	A	$A - B - E_1 - \frac{1}{2}(k^2-1)\Gamma_{\text{reg}}$
		even		$A - \frac{1}{2}k^2\Gamma_{\text{reg}}$
$\{3^4.6\}$	$\mathcal{C}_6$	odd	$A + 2k^2\Gamma_{\text{reg}}$	$A - B - E_1 - \frac{1}{2}(k^2-1)\Gamma_{\text{reg}}$
		even		$A - \frac{1}{2}k^2\Gamma_{\text{reg}}$
$\{3^3.4^2\}$	$\mathcal{C}_2$	odd	$A + 2k^2\Gamma_{\text{reg}}$	$2A - 2B - \frac{1}{2}(k^2-1)\Gamma_{\text{reg}}$
		even		$A - \frac{1}{2}k^2\Gamma_{\text{reg}}$
$\{3^2.4.3.4\}$	$\mathcal{C}_4$	odd	$A + 2k^2\Gamma_{\text{reg}}$	$A - E - \frac{1}{2}(k^2-1)\Gamma_{\text{reg}}$
		even		$A - \frac{1}{2}k^2\Gamma_{\text{reg}}$
$\{3.4.6.4\}$	$\mathcal{C}_6$	odd	$A + k^2\Gamma_{\text{reg}}$	$A - k^2\Gamma_{\text{reg}}$
		even		
$\{3.6.3.6\}$	$\mathcal{C}_6$	odd	$2A + E_2 + \frac{1}{2}(k^2-1)\Gamma_{\text{reg}}$	$A - B - E_1 - \frac{1}{2}(k^2-1)\Gamma_{\text{reg}}$
		even	$A + \frac{1}{2}k^2\Gamma_{\text{reg}}$	$A - \frac{1}{2}k^2\Gamma_{\text{reg}}$
$\{3.12^2\}$	$\mathcal{C}_6$	odd	A	$-2B - 2E_1 - E_2 - \frac{3}{2}(k^2-1)\Gamma_{\text{reg}}$
		even		$A - \frac{3}{2}k^2\Gamma_{\text{reg}}$
$\{4.6.12\}$	$\mathcal{C}_6$	odd	A	$A - 3k^2\Gamma_{\text{reg}}$
		even		
$\{4.8^2\}$	$\mathcal{C}_4$	odd	A	$-2B - 2E - \frac{3}{2}(k^2-1)\Gamma_{\text{reg}}$
		even		$A - \frac{3}{2}k^2\Gamma_{\text{reg}}$

3.2. Discussion

Table 10 shows interesting systematics for single-link and double-link hinged tilings. In the case of single-link hinges, the mobility representation $\Gamma(m) - \Gamma(s)$ is strictly positive in that all the single-link hinged tilings have at least one symmetry detectable mechanism, and

none have a symmetry-detectable state of self-stress. In four cases, one regular ($\{6^3\}$) and three Archimedean ($\{3.12^2\}$, $\{4.6.12\}$, and $\{4.8^2\}$), there is a unique symmetry-detectable mechanism, which is non-degenerate and in fact totally symmetric. Hence, by the symmetry criterion for equiauxeticity discussed above, all four of these frameworks are detectably equiauxetic, giving us three new single-link cases.

3.3. Finiteness of Mechanisms

Furthermore, we claim that in each case, the detected equiauxetic mechanism extends to a finite motion. The interesting cases are those where the mobility representation is exactly $\Gamma(m) - \Gamma(s) = \Gamma_0$, where Γ_0 is the totally symmetric representation in the point group. In such a case, we can argue that the predicted totally symmetric mechanism is not blocked by an equisymmetric state of self-stress (SOSS) and, hence, is finite and equiauxetic. We can characterise each SOSS by assigning a scalar to every bar to represent the tension in that bar. Proof that the equiauxetic mode is finite follows case by case.

Theorem 1. *Single-link hinged versions of the tilings* $\{6^3\}$, $\{3.12^2\}$, $\{4.6.12\}$ *and* $\{4.8^2\}$ *each give an equiauxetic framework supporting a unique, totally symmetric, finite equiauxetic mode.*

Proof. In each case, we consider a configuration close to the original closed arrangement, as pictured in the central column of Figure 1. 'Close' here implies that this configuration occurs before the system reaches any 'special' configurations, where, for instance, sets of bars become aligned. If the chosen configuration can be shown not to have a state of self-stress, then the infinitesimal mechanism that is detected must extend to a finite path.

Case 1. Consider the $\{3.12^2\}$ single-link tiling in Table 7. If there were equal tensions in all bars connecting to a triangular tile, that tile would not be in equilibrium until the motion had reached the 'special' fully extended configuration with all bars directed radially from the triangle centre. We could assign zero tension to these bars, but that would require zero tension in all bars attached to any neighbouring dodecagonal tile, as this tile has alternating constraints connecting it to triangular and dodecagonal tiles. Therefore, the SOSS would have a zero scalar on every bar and would be the null vector. Thus, the equiauxetic mechanism is finite.

Case 2. For tiling $\{4.6.12\}$ in Table 8, the argument is similar but slightly more involved. If a hexagonal tile is in equilibrium, then the bars linking this tile to dodecagonal neighbours all have the same sign, and hence the bars linking hexagonal to square tiles have the opposite sign. If the square tiles are in equilibrium, then all bars to the dodecagonal tiles carry the same sign, and hence, *those* tiles cannot be in equilibrium. Thus, the equiauxetic mechanism is finite.

Case 3. A similar argument applies to the tiling $\{4.8^2\}$, in Table 9, established by requiring equilibrium of square and then octagonal tiles. Hence, the motion is finite in this case too.

Case 4. Of the regular tilings, the hexagonal tiling $\{6^3\}$ also has $\Gamma(m) - \Gamma(s)$ equal to a single copy of the totally symmetric representation. The argument here is simple, in that all bars are equivalent, so if any one bar is in tension, equilibrium is impossible [19]. Hence, all cases (1) to (4) have finite equiauxetic mechanisms. □

In summary, there are four cases where the single-link frameworks have $\Gamma(m) - \Gamma(s)$ equal to A, implying a single, equiauxetic mode for all choices of unit cells. These are $\{6^3\}$, $\{3.12^2\}$, $\{4.6.12\}$, and $\{4.8^2\}$. The regular $\{6^3\}$ was treated in [19]. Here, we have identified three more equiauxetic frameworks by extending symmetry counting calculations to single-link hinged Archimedean tilings.

4. Double-Link Hinged Tilings

We also consider here the double-link analogue of the hinged structures discussed above. These have been described before for regular tilings [19], and an example of the construction for doubling up on the number of links is shown in Figure 3.

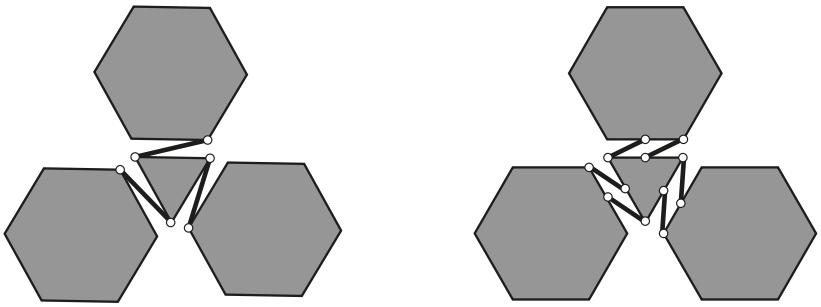

Figure 3. Single-link (**a**) and double-link (**b**) versions of the hinged tilings. A sample of the auxetic expansion mode for $\{3.6.3.6\}$, the Kagome lattice, is shown here. A similar construction can be applied to any of the systems illustrated in Figure 1. The extra constraint imposed by the double link made up of bars of the same length implies that the edges of linked tiles remain pairwise parallel, as in the unexpanded system.

For double-link hinged tilings, the mobility count is again given by the trace of Equation (3) under the identity,

$$m - s = 3n - 2b + 1$$

as $\chi_T(E) = 2$ and $\chi_R(E) = 1$ in 2D, and n counts the bodies (tiles) as before, but now two bars are associated with each of the b edges in the unit cell. In the double-link case, the site symmetry of any individual bar constraint is the trivial C_1.

Calculations and Discussion

The mobility calculation for the double-link version of a hinged tiling is identical to that for the single-link in all but one respect. There are now two constraints per edge of the original tiling, and there is no symmetry element preserving a constraint. The permutation representation $\Gamma(e, C)$ now has $\chi(E)$ equal to twice the value for the single-link version, but zero under all other operations, i.e., it is a multiple of Γ_{reg}. Hence, $\Gamma(m) - \Gamma(s)$ is available by a simple modification of the tabulated character calculations for the single-link case.

The results for the modified calculation have already been given in the final column of Table 10. For the single-link hinge tilings, many cases have mechanisms in addition to the totally symmetric expansion that is present in all cases. The double-link version is overconstrained according to the scalar count in almost all cases. (The exceptions are the zero counts for $\{4^4\}$ and $\{3^3.4^2\}$ with $k = 1$). In the symmetry counts, the same overconstraint is shown in the reducible representation $\Gamma(m) - \Gamma(s)$ for general values of k, which typically includes a positive multiple of the totally symmetric representation A balanced against a negative multiple of the regular representation proportional either to k^2 or $(k^2 - 1)$. Hence, the totally symmetric representation A appears in $\Gamma(m) - \Gamma(s)$ with zero or negative weight in most cases. The exceptions, where the sole symmetry-detectable mechanism is of A symmetry, are the four double-link hinged frameworks with $k = 1$ based on $\{6^3\}$, $\{3^4.6\}$, $\{3^2.4.3.4\}$, and $\{3.6.3.6\}$. The regular case $\{6^3\}$ was treated in [19]. Here, we have identified three more equiauxetic frameworks by extending symmetry counting calculations to the double-link hinged Archimedean tilings.

We can show that the equiauxetic modes in these cases are finite mechanisms.

Theorem 2. *Double-link hinged versions of the tilings* $\{6^3\}$, $\{3^4.6\}$, $\{3^2.4.3.4\}$ *and* $\{3.6.3.6\}$ *(all with* $k = 1$*) each give an equiauxetic framework supporting a unique, totally symmetric, finite equiauxetic mode.*

Proof. We start by establishing two symmetry conditions. Condition (1): Consider an n-gon of the tiling that has an n-fold axis of symmetry through its centre. For such a polygon, all n edge pairs must have the same member forces $\boldsymbol{S}_1$ and $\boldsymbol{S}_2$ (call this, for simplicity, a type-1 n-gon). For a type-1 polygon, n rotated copies of $\boldsymbol{S}_1$, and $\boldsymbol{S}_2$ can only give equilibrium if each resultant $\boldsymbol{S}$ of $\boldsymbol{S}_1$ and $\boldsymbol{S}_2$ passes through the centre of the n-gon. (This is always possible for some values of $\boldsymbol{S}_1$ and $\boldsymbol{S}_2$ if the two links are not collinear.). Since $\boldsymbol{S}_1$ and $\boldsymbol{S}_2$ are parallel, their resultant is also parallel with them. Near to the initial configuration, however, the resultant cannot pass through the centre of the other (connected) polygon. Condition (2): Any pair of links on a C_2-element enforces $\boldsymbol{S}_1 = \boldsymbol{S}_2 = \boldsymbol{S}/2$, and $\boldsymbol{S}$ runs along the midline of $\boldsymbol{S}_1$ and $\boldsymbol{S}_2$.

Now we look at the tilings case by case.

Case 1. $\{6^3\}$: Condition (2) forces each $\boldsymbol{S}$ to be parallel with its pair of links and not passing through the centres of connected hexagons, 6-fold symmetry implies six resultant forces representing the same moment about the centre of the hexagon, and hence, equilibrium is not possible with non-zero forces in links in this case.

Case 2. $\{3.6.3.6\}$: Both the hexagons and triangles are of type 1, so any resultant $\boldsymbol{S}$ should be directed through the centres of the connected hexagon and triangle, which is not possible in a general configuration near to the initial closed configuration.

Case 3. $\{3^2.4.3.4\}$: Consider the double-link analogue of Figure 1a(ii). Since both the hexagon and the central triangle (with a C_3 axis in its centre) are of type 1, the resultant of forces around the hexagon (call it $\boldsymbol{S}_6$) and any non-zero resultant of forces around the central triangle (call this $\boldsymbol{S}_3$) must go through their respective face centres. Now, any non-central triangle must be balanced by a copy of $\boldsymbol{S}_3$ and $\boldsymbol{S}_6$, as well as by the third resultant S represented by the pair on a C_2 axis. Close to the initial state, however, it is impossible for these to be concurrent since the intersection of $\boldsymbol{S}_3$ and $\boldsymbol{S}_6$ is outside the triangle, just beyond its vertex in front of the C_2 axis, while S passes that C_2 axis and is nearly parallel to the edges on which S acts. Hence, equilibrium is not possible with non-zero forces in links in this case.

Case 4. $\{3^2.4.3.4\}$: Consider the double-link analogue of Figure 1c(ii). Since squares are of type 1, all resultants of $\boldsymbol{S}_4$ are equal and pass through the centres of their respective faces. Now, close to the initial configuration, any pair of triangles sharing a C_2 axis is surrounded by four copies of $\boldsymbol{S}_4$ that have a moment with the same sense about the shared C_2 axis. Hence, equilibrium is not possible with non-zero forces in links in this case. □

An animation of the equiauxetic mode for the double-link hinged Kagome framework ($\{3.6.3.6\}$) is available as file S1 Kagome.mp4 in the Supplementary Material for this article.

5. Conclusions

The analysis reported here has illustrated the power of applying symmetry to the mobility criteria for periodic frameworks. The extension from pure counting to counting-with-symmetry typically leads to stronger necessary conditions for motion. Here, we have shown that the extended count given by the master equation for periodic body-bar frameworks (3), combined with the criterion for equiauxeticity from Section 2.2, allows us to detect generic equiauxetic behaviour in plausible models of 2D materials and metamaterials based on the canonical Archimedean tilings of the plane.

The main result of this analysis is the identification of two new sets of equiauxetic 2D frameworks, one set emerging from tilings with single links and the other from tilings with double links.

For single-link frameworks of the type shown in Figure 1, scalar counting shows that all are underconstrained. The symmetry-extended calculation shows that every framework has at least one totally symmetric, equiauxetic mode, and it detects no states of self-stress. Exactly four of the regular and Archimedean tilings generate equiauxetic single-link frameworks. These are $\{3.12^2\}$, $\{4.6.12\}$, and $\{4.8^2\}$, and the previously identified [19] regular hexagonal case $\{6^3\}$.

In contrast, double-link frameworks of the type shown in Figure 3b are typically overconstrained, as the scalar counts for $k = 1$ show for all but $\{3.6\}$, $\{4^4\}$ and $\{3^3.4^2\}$. The application of symmetry reveals that these counts mask the existence of a totally symmetric equiauxetic mode for $k = 1$, for all but $\{3.12^2\}$ and $\{4.8^2\}$. In four cases, the only mechanism detected by symmetry is the totally symmetric equiauxetic mode, and hence these are equiauxetic frameworks. These are $\{3^4.6\}$, $\{3^2.4.3.4\}$, $\{3.6.3.6\}$, and the previously identified [19] regular hexagonal case $\{6^3\}$.

Counting arguments for mobility lead to necessary rather than sufficient conditions as they relate to a difference, not an absolute value. This is true of scalar counting and is still true of counting with symmetry. Addition of an equal number of mechanisms and states of self-stress does not change $m - s$, and addition of *equisymmetric* sets of mechanisms and states of self-stress (i.e., sets that transform in the same way under all symmetry operations of the framework) does not affect $\Gamma(m) - \Gamma(s)$. In this connection, an interesting observation from the calculations reported here concerns the single-link hinged tilings $\{6^3\}$ and $\{3.12^2\}$. The same scalar count of $m - s = 1$ independently of k holds for both because the triangles in the interstices between the 12-gons add $2k^2 \times 3$ to the count of freedoms, but this is cancelled by the $6k^2$ constraints imposed by the bars that connect to the triangles. In the character table calculation of the symmetry $\Gamma(m) - \Gamma(s)$, the scalar count implies that the character under the identity operation is the same for the single-link hinged tilings $\{6^3\}$ and $\{3.12^2\}$. The triangles of $\{3.12^2\}$ lie on C_3 axes, and hence the $\Gamma(v, C)$ has character 3 under the associated operations, but this does not contribute to $\Gamma(m) - \Gamma(s)$ as the character of the rigid body modes is zero for this operation. In effect, the contact polyhedron for $\{3.12^2\}$ can be reduced to that of $\{6^3\}$ and by removing the vertices and edges associated with the triangles without affecting $\Gamma(m) - \Gamma(s)$. The missing tiles can be reinstated with an appropriate rotation for any configuration of the framework.

Although the examples in Figure 1 refer to equilateral tiles, the symmetry calculations would be the same for a wider class of systems. For example, subject to retention of symmetry, edge lengths might be modified or gaps might be introduced between tiles, and indeed, the precise geometry of the single and double links has not been specified here beyond the restrictions imposed by symmetry.

It is also interesting to compare the present study with results on the mobility of tilings constructed under different physical models. In [7,16,18], Archimedean tilings are included amongst examples of bar-and-joint frameworks defined in a different way by considering the edges of the tiles as a bar-joint network rather than considering the tiles as rigid-bodies—that model also generates equiauxetic frameworks of a different kind.

Other directions for future work suggested by the present investigation include physical modelling of the systems studied here and extension of the symmetry techniques to 3D. Reproduction of pin-jointed frameworks with 3D printing techniques is problematic, but by introducing elasticity and replacing the pin joints with 'elastic joints', it should be possible to study the resulting compliant mechanisms in physical models produced by this technology. Extension of our symmetry reasoning to the design of auxetics and equiauxetics in 3D is also a compelling future direction for this research area. We believe that the symmetry approach has much to offer in terms of generating ideas for new metamaterials and in analysing the performance of systems of this type.

Supplementary Materials: The following supporting information can be downloaded at: https://www.mdpi.com/article/10.3390/sym14020232/s1 One animation file (Video S1 Kagome.mp4) is available.

Author Contributions: Conceptualization, T.T., P.W.F., S.D.G. and F.K.; methodology, T.T., P.W.F., S.D.G. and F.K.; validation, T.T., P.W.F., S.D.G. and F.K.; visualization, T.T., P.W.F., S.D.G. and F.K.; formal analysis, T.T., P.W.F., S.D.G. and F.K.; investigation, T.T., P.W.F., S.D.G. and F.K.; writing—original draft preparation, T.T., P.W.F., S.D.G. and F.K.; writing—review and editing, T.T., P.W.F., S.D.G. and F.K. All authors have read and agreed to the published version of the manuscript.

Funding: This work was supported in part by NKFIH under grants K 119440 (T.T. and F.K.), K 128584 (F.K.) and TPK2020 BME-NCS (F.K.).

Conflicts of Interest: The authors declare no conflict of interest. The funders had no role in the design of the study; in the collection, analyses, or interpretation of data; in the writing of the manuscript, or in the decision to publish the results.

References

1. Ren, X.; Das, R.; Tran, P.; Ngo, T.D.; Xie, Y.M. Auxetic metamaterials and structures: A review. *Smart Mater. Struct.* **2018**, *27*, 023001. [CrossRef]
2. Yang, W.; Li, Z.-M.; Shi, W.; Xie, B.-H.; Yang, M.-B. Review on auxetic materials. *J. Mater. Sci.* **2004**, *39*, 3269–3279. [CrossRef]
3. Evans, K.E.; Alderson, A. Auxetic Materials: Functional Materials and Structures from Lateral Thinking! *Adv. Mater.* **2000**, *12*, 617–628. [CrossRef]
4. Lakes, R.S. Negative-Poisson's-Ratio Materials: Auxetic Solids. *Annu. Rev. Mater. Res.* **2017**, *47*, 63–81. [CrossRef]
5. Lim, T. *Auxetic Materials and Structures*; Engineering Materials; Springer: Singapore, 2014.
6. Hu, H.; Zhang, M.; Liu, Y. *Auxetic Textiles*; The Textile Institute Book Series; Elsevier Science: Amsterdam, The Netherlands, 2019.
7. Mitschke, H.; Robins, V.; Mecke, K.; Schröder-Turk, G.E. Finite auxetic deformations of plane tessellations. *Proc. R. Soc. A Math. Phys. Eng. Sci.* **2013**, *469*, 20120465. [CrossRef]
8. Borcea, C.S.; Streinu, I. Periodic frameworks and flexibility. *Proc. R. Soc. A Math. Phys. Eng. Sci.* **2010**, *466*, 2633–2649. [CrossRef]
9. Lakes, R.S. Foam Structures with a Negative Poisson's Ratio. *Science* **1987**, *235*, 1038–1040. [CrossRef]
10. Evans, K.E. Auxetic polymers: A new range of materials. *Endeavour* **1991**, *15*, 170–174. [CrossRef]
11. Grima, J.N.; Evans, K.E. Auxetic behaviour from rotating squares. *J. Mater. Sci.* **2000**, *19*, 1563–1565.
12. Grima, J.N.; Alderson, A.E.; Evans, K.E. Auxetic behaviour from rotating rigid units. *Phys. Status Solidi* **2005**, *242*, 561–575. [CrossRef]
13. Attard, D.; Grima, J.N. Auxetic behaviour from rotating rhombi. *Phys. Status Solidi* **2008**, *245*, 2395–2404. [CrossRef]
14. Mizzi, L.; Azzopardi, K.M.; Attard, D.; Grima, J.N.; Gatt, R. Auxetic metamaterials exhibiting giant negative Poisson's ratios. *Phys. Status Solidi (RRL)—Rapid Res. Lett.* **2015**, *9*, 425–430. [CrossRef]
15. Mizzi, L.; Azzopardi, K.M.; Gatt, R.; Farrugia, P.S.; Grima, J.N. An analytical and finite element study on the mechanical properties of irregular hexachiral honeycomb. *Smart Mater. Struct.* **2018**, *27* 105116. [CrossRef]
16. Mitschke, H.; Schröder-Turk, G.E.; Mecke, K.; Fowler, P.W.; Guest, S.D. Symmetry detection of auxetic behaviour in 2D frameworks. *EPL Europhys. Lett.* **2013**, *102*, 66005. [CrossRef]
17. Guest, S.D.; Fowler, P.W. Symmetry-extended counting rules for periodic frameworks. *Philos. Trans. R. Soc. A Math. Phys. Eng. Sci.* **2014**, *372*, 20120029. [CrossRef]
18. Mitschke, H. Deformations of Skeletal Structures. Master's Thesis, Universität Erlangen-Nürnberg, Erlangen, Germany, 2009.
19. Fowler, P.W.; Guest, S.D.; Tarnai, T. Symmetry Perspectives on Some Auxetic Body-Bar Frameworks. *Symmetry* **2014**, *6*, 368–382. [CrossRef]
20. Novoselov, K.S.; Jiang, D.; Schedin, F.; Booth, T.J.; Khotkevich, V.V.; Morozov, S.V.; Geim, A.K. Two-dimensional atomic crystals. *Proc. Natl. Acad. Sci. USA* **2005**, *102*, 10451–10453. [CrossRef]
21. Zhang, S.; Zhou, J.; Wang, Q.; Chen, X.; Kawazoe, Y.; Jena, P. Penta-graphene: A new carbon allotrope. *Proc. Nat. Acad. Sci. USA* **2015**, *112*, 2372–2377. [CrossRef]
22. Einollahzadeh, H.; Fazeli, S.M.; Dariani, R.S. Studying the electronic and phononic structure of penta-graphene. *Sci. Technol. Adv. Mater.* **2016**, *17*, 610–617. [CrossRef]
23. Gu, Q.; Xing, D.; Sun, J. Superconducting Single-Layer T-Graphene and Novel Synthesis Routes. *Chin. Phys. Lett.* **2019**, *36*, 097401. [CrossRef]
24. Suzuki, Y.; Cardone, G.; Restrepo, D.; Zavattieri, P.D.; Baker, T.S.; Tezcan, F.A. Self-assembly of coherently dynamic, auxetic, two-dimensional protein crystals. *Nature* **2016**, *533*, 363–373. [CrossRef] [PubMed]
25. Flores, A. Hinged Tilings. *N. Am. GeoGebra J.* **2017**, *6*, 1–11.
26. Attard, D.; Farrugia, P.S.; Gatt, R.; Grima, J.N. Starchirals: A novel class of auxetic hierarchal structures. *Int. J. Mech. Sci.* **2020**, *179*, 105631. [CrossRef]

27. dos Santos, F.A.; Favata, A.; Micheletti, A.; Paroni, R. Design of auxetic plates with only one degree of freedom. *Extrem. Mech. Lett.* **2021**, *42*, 101091. [CrossRef]
28. Mizzi, L.; Spaggiari, A. Chiralisation of Euclidean polygonal tessellations for the design of new auxetic metamaterials. *Mech. Mater.* **2021**, *153*, 103698. [CrossRef]
29. Grünbaum, B.; Shephard, G.C. *Tilings and Patterns*; Dover Books on Mathematics Series; Dover Publications: Mineola, NY, USA, 2013.
30. Kovács, F.; Tarnai, T.; Fowler, P.W.; Guest, S.D. A class of expandable polyhedral structures. *Int. J. Solids Struct.* **2004**, *41*, 1119–1137. [CrossRef]
31. Kovács, F.; Tarnai, T.; Guest, S.D.; Fowler, P.W. Double-link expandohedra: A mechanical model for expansion of a virus. *Proc. R. Soc. Lond. Ser. A Math. Phys. Eng. Sci.* **2004**, *460*, 3191–3202. [CrossRef]
32. Speir, J.A.; Munshi, S.; Wang, G.; Baker, T.S.; Johnson, J.E. Structures of the native and swollen forms of cowpea chlorotic mottle virus determined by X-ray crystallography and cryo-electron microscopy. *Structure* **1995**, *3*, 63–78. [CrossRef]
33. Zhang, X.; Sheng, J.; Plevka, P.; Kuhn, R.J.; Diamond, M.S.; Rossmann, M.G. Dengue structure differs at the temperatures of its human and mosquito hosts. *Proc. Nat. Acad. Sci. USA* **2013**, *110*, 6795–6799. [CrossRef]
34. Tay, T.-S. Rigidity of multi-graphs. I. Linking rigid bodies in n-space. *J. Comb. Theory Ser. B* **1984**, *36*, 95–112. [CrossRef]
35. Guest, S.; Schulze, B.; Whiteley, W.J. When is a symmetric body-bar structure isostatic? *Int. J. Solids Struct.* **2010**, *47*, 2745–2754. [CrossRef]
36. Guest, S.D.; Fowler, P.W. A symmetry-extended mobility rule. *Mech. Mach. Theory* **2005**, *40*, 1002–1014. [CrossRef]
37. Blatov, V.A.; O'Keeffe, M.; Proserpio, D.M. Vertex-, face-, point-, Schläfli-, and Delaney-symbols in nets, polyhedra and tilings: Recommended terminology. *CrystEngComm* **2010**, *12*, 44–48. [CrossRef]
38. Coxeter, H. *Regular Polytopes*; Dover Books on Advanced Mathematics; Dover Publications: Mineola, NY, USA, 1973.
39. Atkins, P.W.; Child, M.S.; Phillips, C.S.G. *Tables for Group Theory*; Oxford University Press: Oxford, UK, 1970.
40. Altmann, S.L.; Herzig, P. *Point-Group Theory Tables*; Clarendon Press: Oxford, UK, 1994.
41. Bishop, D.M. *Group Theory and Chemistry*; Dover Publications: Mineola, NY, USA, 1993.
42. Fowler, P.W.; Guest, S.D. A symmetry extension of Maxwell's rule for rigidity of frames. *Int. J. Solids Struct.* **2000**, *37*, 1793–1804. [CrossRef]
43. Kangwai, R.; Guest, S. Detection of finite mechanisms in symmetric structures. *Int. J. Solids Struct.* **1999**, *36*, 5507–5527. [CrossRef]